Research Article
L^1TV Computes the Flat Norm for Boundaries

Simon P. Morgan and Kevin R. Vixie

We show that the recently introduced L^1TV functional can be used to explicitly compute the flat norm for codimension one boundaries. Furthermore, using L^1TV, we also obtain the flat norm decomposition. Conversely, using the flat norm as the precise generalization of L^1TV functional, we obtain a method for denoising nonboundary or higher codimension sets. The flat norm decomposition of differences can made to depend on scale using the *flat norm with scale* which we define in direct analogy to the L^1TV functional. We illustrate the results and implications with examples and figures.

1. Introduction

In this research announcement, we point out that the L^1TV functional, introduced and studied in the continuous setting in [1–4] and earlier in the discrete setting in [5, 6], provides a convenient way of computing both the value of, and the optimal decomposition required by, the *flat norm* from geometric measure theory.

The L^1TV functional was introduced as an improvement to the now-classic Rudin-Osher-Fatemi total variation-based denoising [7]. Among its many nice properties is the way it handles binary images, making it useful for shape processing. Theoretically speaking, the clean geometric structure of the functional and its minimizers is very attractive (see [2, 3] for details).

Joan Glaunès was, as far as we know, the first to suggest and use the *flat norm* from geometric measure theory as a distance in shape space. In his dissertation [8] and a couple of application papers [9, 10] with collaborators, the dual formulation of the flat norm is used to compute distances between shapes.

2. L^1TV gives the flat norm

The L^1TV functional introduced and studied in [1] is given by

$$F(u) = \int_{\mathbb{R}^n} |\nabla u|\, dx + \lambda \int_{\mathbb{R}^n} |u - u_0|\, dx, \tag{2.1}$$

where u and u_0 are functions from $\mathbb{R}^n$ to $\mathbb{R}$ with u_0 being the input function. In image analysis applications, n is usually 2 and u_0 is the measured image intensity function. The optimal u minimizing (2.1) can be thought of as a *denoised* version of u_0. Typically, one chooses the parameter λ based on noise levels since this choice selects the scale below which features or oscillations are ignored. In the case that the input function is binary, Chan and Esedoglu observe that the functional reduces to

$$F_{\mathrm{CE}}^\lambda(\Sigma) = \mathrm{Per}(\Sigma) + \lambda |\Sigma \triangle \Omega|, \tag{2.2}$$

where the binary minimizer is χ_Σ, the binary input is χ_Ω, $\mathrm{Per}(\Sigma)$ is the perimeter of Σ, and $\triangle$ denotes the symmetric difference. Of course χ_E denotes the characteristic function on E, with a value of 1 on E and 0 on the complement of E. Now, let $\Sigma(\Omega,\lambda)$ be a binary minimizer of (2.2), that is,

$$\Sigma(\Omega,\lambda) \equiv \arg\min F_{\mathrm{CE}}^\lambda(\Sigma) = \mathrm{Per}(\Sigma) + \lambda |\Sigma \triangle \Omega|. \tag{2.3}$$

For our convenience, we record the optimal decomposition of Ω into $\{\Sigma(\Omega,\lambda)$ and $(\Sigma(\Omega,\lambda) \triangle \Omega)\}$ as the pair $\{\partial\Omega, \Sigma(\Omega,\lambda) \triangle \Omega\}$.

In what follows, we use the notions of *current*, *mass*, and ∂ and supporting ideas from geometric measure theory. We introduce and explain these in some detail in the Appendix. Informally, one can gain much by thinking of the *n-current* T_E as an orientable n-submanifold or n-rectifiable set $E \subset \mathbb{R}^{n+k}$ with an orientation, of the *mass* $M(T_E)$ as the n-dimensional volume of E, and of ∂T, the boundary of T, as the oriented boundary of E with orientation imposed by the orientation of E. We sometimes omit the subscript indicating the support of the current, referring to currents T and S. For those without experience with currents, we suggest focusing on the examples in the Appendix.

The *flat norm* of an n-current T, denoted by $\mathbb{F}(T)$, is given by

$$\mathbb{F}(T) \equiv \min_S \{\mathbf{M}(S) + \mathbf{M}(T - \partial S)\}, \tag{2.4}$$

where S varies over $n+1$-currents and $\mathbf{M}$ is the *mass* of the indicated currents. We refer to $\{T,S\}$ as the flat norm induced, optimal decomposition. Now we get the following results.

THEOREM 2.1. *For the current $T_{\partial\Omega}$,*

$$\mathbb{F}(T_{\partial\Omega}) = F_{\mathrm{CE}}^1(\Sigma(\Omega,1)),$$

and

$$\{T_{\partial\Omega}, S_{\Sigma(\Omega,1)\triangle\Omega}\} \tag{2.5}$$

is the optimal decomposition required by the flat norm.

Theorem 2.1 says that L1TV computes the flat norm. This relation between the flat norm and the L1TV functional immediately suggests a very useful generalization of the flat norm.

Definition 2.2 (Flat norm with scale).

$$\mathbb{F}_\lambda(T) \equiv \min_S \{\lambda \mathbf{M}(S) + \mathbf{M}(T - \partial S)\}. \tag{2.6}$$

Theorem 2.1 is then simply a special case of the next theorem.

THEOREM 2.3. *For the current $T_{\partial\Omega}$,*

$$\mathbb{F}_\lambda(T_{\partial\Omega}) = F_{CE}^\lambda(\Sigma(\Omega,\lambda)),$$

and (2.7)

$$\{T_{\partial\Omega},\ S_{\Sigma(\Omega,\lambda)\triangle\Omega}\}$$

is the optimal decomposition that the flat norm with scale requires.

Proof of Theorem 2.3. The proof consists of a careful checking that the picture one can draw holds after the definitions of *mass* (**M**) and *perimeter* (Per) are used to translate the picture into analytic terms. Very briefly, we have

$$F_{CE}^\lambda(\Sigma) = \lambda|\Sigma \triangle \Omega| + \text{Per}(\Sigma) = \lambda M(S_{\Sigma\triangle\Omega}) + M(T_{\partial\Sigma}) = \lambda M(S_{\Sigma\triangle\Omega}) + M(T_{\partial\Omega} - \partial S_{\Sigma\triangle\Omega}). \tag{2.8}$$

Figure 2.1 illustrates this pictorially. □

Our final observation is that the *flat norm with scale* gives us the same decomposition as we would get if we first scaled T, computed the *flat norm* decomposition, and then reversed the scaling. More precisely, see the following lemma.

LEMMA 2.4. *Denote the optimal $\mathbb{F}_\lambda$ decomposition by $\{T,S\}_\lambda$. Then*

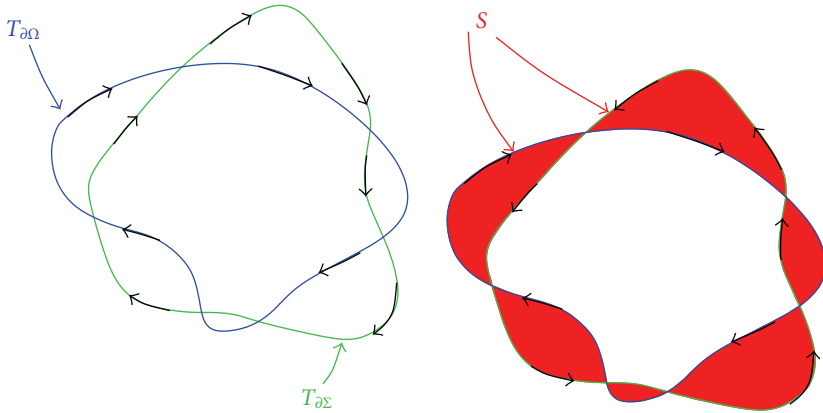$$\{T,S\}_\lambda = d_{1/\lambda\#}\{d_{\lambda\#}(T), d_{\lambda\#}(S)\}_1, \tag{2.9}$$

where d_λ denotes the λ-dilation of $\mathbb{R}^m$, and $d_{\lambda\#}(T_M) = T_{d_\lambda(M)}$.

Proof. The minimizing decomposition $\{T,S\}_\lambda$ which minimizes $\lambda \mathbf{M}(S) + \mathbf{M}(T - \partial S)$ also minimizes $\lambda^n \mathbf{M}(S) + \lambda^{n-1} \mathbf{M}(T - \partial S) = \mathbf{M}(d_{\lambda\#}S) + \mathbf{M}(d_{\lambda\#}(T - \partial S))$. Therefore, to get the minimizer for $\mathbb{F}_\lambda$ run the optimization required by $\mathbb{F}_1$ using $d_{\lambda\#}(T)$ as input, and then contract with $d_{1/\lambda\#}$. □

We now discuss applications and examples with pictures which should clarify things for those with less exposure to geometric measure theory.

3. Applications and illustrating examples

The value of the above results is fully realized by exploring their use in applications to images and shapes. As observed by Glaunès and others, the flat norm is a very natural candidate for distances between shapes. We now very briefly explore and illustrate applications of the above observations.

$$T_{\partial \Sigma} = T_{\partial \Omega} - \partial S_{\Sigma \triangle \Omega},$$
$$F_{CE}^{\lambda}(\Sigma) = \lambda |\Sigma \triangle \Omega| + \mathrm{Per}(\Sigma),$$
$$= \lambda M(S_{\Sigma \triangle \Omega}) + M(T_{\partial \Sigma})$$
$$= \lambda M(S_{\Sigma \triangle \Omega}) + M(T_{\partial \Omega} - \partial S_{\Sigma \triangle \Omega}).$$

Figure 2.1. In this figure we illustrate the translation of the L^1TV view to the flat norm view. The perimeter of Σ becomes the mass of $T_{\partial \Omega} - \partial S_{\Sigma \triangle \Omega}$ and the volume of $\Sigma \triangle \Omega$ becomes the mass of $S_{\Sigma \triangle \Omega}$. Note: this figure does not depict a minimizer. Rather, we depict Ω and any candidate Σ.

3.1. Generalized flat norm: flat norm with scale. As mentioned in Section 2, by letting the $\lambda \neq 1$, one has a natural way to vary the intrinsic scale in the flat norm

$$\mathbb{F}_{\lambda}(T_{\partial E}) \equiv \min_{S} \{\lambda \mathbf{M}(S) + \mathbf{M}(T_{\partial E} - \partial S)\} = F_{CE}^{\lambda}(E), \tag{3.1}$$

where $T_{\partial E}$ represents ∂E. The main point here is that this is easy to compute, given the connection to the L^1TV functional. Varying λ gives us the ability to choose what scale is big and worth keeping. See Figure 3.1.

3.2. Flat norm via L^1TV. We can use the L^1TV functional to very easily calculate *both* the flat norm of differences between surfaces which are boundaries *and* the optimal decomposition of that difference into surface and area parts. In Figure 3.2, the decomposition of a boundary current $T_{\partial \Omega}$ into the diminished boundary $T_{\partial \Sigma}$ and the symmetric difference current $S_{\Sigma \triangle \Omega}$ is illustrated.

3.3. L^1TV by the dual form of the flat norm. The dual formulation of the flat norm can be used to compute L^1TV minimizers. In what follows, we define spt T to be the support of T. The following results establish that maximizing forms, or in some cases, maximizing sequences of forms, contain the decomposition into S and $T - \partial S$.
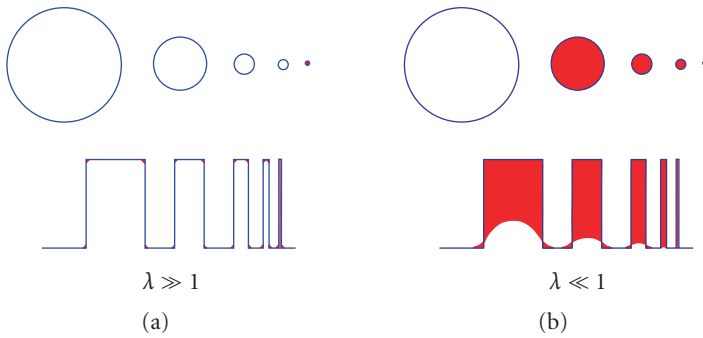
Figure 3.1. Flat norm with scale decompositions as a function of λ: the larger λ is, the less smoothing there is. Let T denote the blue input 1-currents and S denote the red optimal 2-currents. Then in fact, λ is the bound on the curvature allowed in $T - \partial S$, see [3, 2] for details. Accordingly, the curves $T - \partial S$ are allowed greater curvature in the curves on the left than is permitted in those on the right.
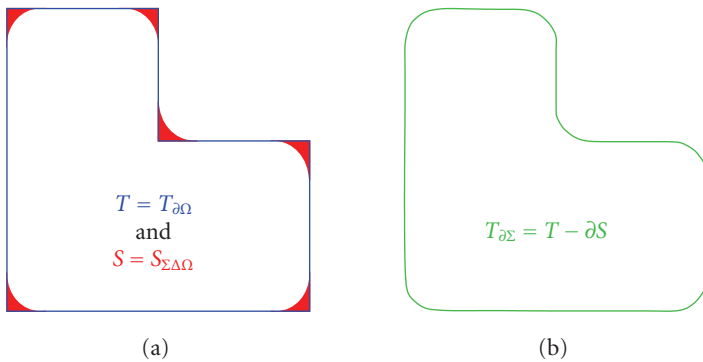

Figure 3.2. A simple reinterpretation of the L^1TV input and minimizer gives us the flat norm of $T_{\partial\Omega}$ and the decomposition into the diminished boundary $T_{\partial\Sigma}$ and the symmetric difference current $S_{\Sigma\Delta\Omega}$.

PROPOSITION 3.1. *Suppose that* $T(\phi) = F(T) = \min_S(M(S) + M(T - \partial S))$, *where* ϕ *is a smooth, compactly supported n-form satisfying* $|\phi| \leq 1, |d\phi| \leq 1$, *and* T *is an n-rectifiable current with density* $\Theta = 1$ $\mathcal{H}^n$ *almost everywhere on* $\mathrm{spt}\, T$, *then on the support of S,* $|d\phi| = 1$, *and on the support of* $T - \partial S$, $|\phi| = 1$.

Proof. For a minimizing choice of S, we have that

$$
\begin{aligned}
T(\phi) &= F(T) = M(S) + M(T - \partial S), \\
T(\phi) &= \partial S(\phi) + (T - \partial S)(\phi), \\
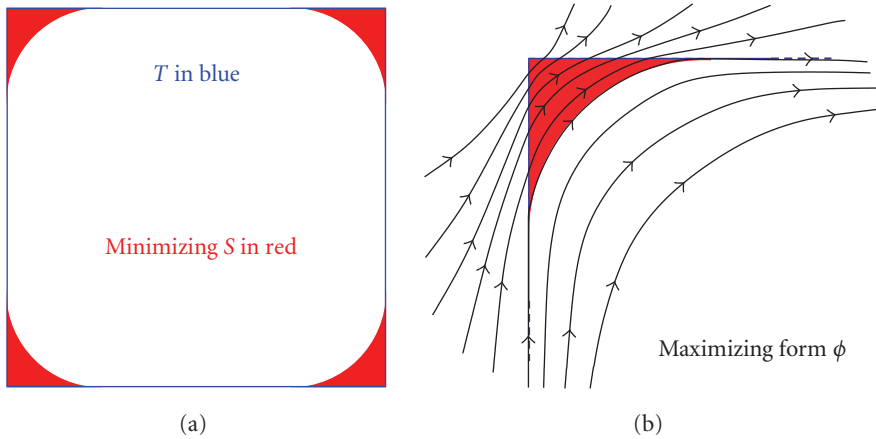\partial S(\phi) &= S(d\phi),
\end{aligned}
\tag{3.2}
$$

Figure 3.3. Example of a maximizing form for a square T as input. On the right-hand side of the figure, details of the form are shown. We visualize the form as a vector field. On $T - \partial S$, $|\phi| = 1$ everywhere and on S (red), $|d\phi| = 1$ everywhere, while off of these sets, both $|\phi| < 1$ and $|d\phi| < 1$.

so that

$$S(d\phi) + (T - \partial S)(\phi) = M(S) + M(T - \partial S). \tag{3.3}$$

We know that $M(S) = \int 1 d\mathcal{H}^{n+1} \llcorner \operatorname{spt} S$ and $M(S) = \int < d\phi, \vec{S} > d\mathcal{H}^{n+1} \llcorner \operatorname{spt} S$, $|\vec{S}| = 1$ and $|d\phi| \leq 1$ on $\operatorname{spt} S$. Similarly for $T - \partial S$. We immediately get that $|\phi| = 1$, $\mathcal{H}^n \llcorner \operatorname{spt}(T - \partial S)$ almost everywhere and $|d\phi| = 1$, $\mathcal{H}^{n+1} \llcorner \operatorname{spt} S$ almost everywhere. □

See Figure 3.3 for an example maximizing form. Note that when S is not unique, this proposition implies that $|d\phi| = 1$ on the union of supports of all possible minimizing S's. If we do not have a maximizing form, we have the following modified proposition together with the fact that there will be sequence of forms ϕ_i such that $T(\phi_i) \to_{i \to \infty} F(T)$. This easily yields the following.

PROPOSITION 3.2. *Suppose that $T(\phi_i) \to F(T) = M(S) + M(T - \partial S)$. Then there is a subsequence of ϕ_i, ϕ_{i_k} such that $|\phi_{i_k}| \to 1$ $\mathcal{H}^n \llcorner \operatorname{spt}(T - \partial S)$ almost everywhere and $|d\phi| \to 1$ $\mathcal{H}^{n+1} \llcorner \operatorname{spt} S$ almost everywhere.*

This modified proposition is necessary since there are easily constructed examples having no smooth maximizing form. In fact, the example shown in Figure 3.3 is not actually smooth. The optimizing $d\phi$ we show is actually Lipschitz, so it can be arbitrarily well approximated by smooth forms even though it is not itself smooth. The nonsmoothness originates at the points of $T - \partial S$ where the circular arcs join the sides of the square tangentially. At these points, the boundary is merely $C^{1,1}$.

Remark 3.3. Note that Propositions 3.1 and 3.2 are true if ϕ and $d\phi$ are merely measurable with respect to the measures $\mathcal{H}^n \llcorner \operatorname{spt}(T - \partial S)$ and $\mathcal{H}^{n+1} \llcorner \operatorname{spt} S$.
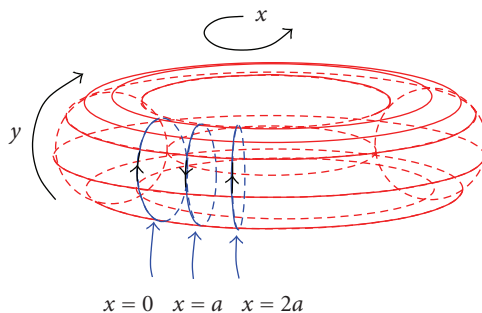
Figure 3.4. The 3 circles example. The metric is chosen so that the circles are parallel to each other. Optimal S can be either the region between the $x = 0$ and $x = a$ circles or the region between the $x = a$ and $x = 2a$ circles.

We now state an outline of a reasonable set of steps that would be very useful for computations using the dual formulation of the flat norm.

CONJECTURE 3.4. *Suppose that T is integer density rectifiable with rectifiable boundary ∂T and that both T and ∂T have finite mass. Define Φ to be the collection of all Lipschitz forms ϕ maximizing $T(\phi)$ and satisfying $|\phi| \leq 1$ and $|d\phi| \leq 1$. Define X to be the closure of the set on which $|d\phi| = 1$ for every $\phi \in \Phi$. Finally, define $\mathbb{S}$ to be the collection of all optimizing currents S such that $\mathbb{F}(T) = M(S) + M(T - \partial S)$. Then*
   (a) *there is an $S \in \mathbb{S}$ such that both S and ∂S are integer density rectifiable,*
   (b) $\Phi \neq \varnothing$,
   (c) $X = \bigcup_{S \in \mathbb{S}} \mathrm{spt}(S)$,
   (d) $|\phi| = 1$ *on* $\mathrm{spt}(T - \partial S)$.

Part (a) says that although we are not constraining the minimizing currents to be rectifiable, there is at least one in the set of minimizers that is rectifiable. Part (b) says that there are always maximizing forms if we permit them to be merely Lipschitz instead of smooth. Part (c) enables us to see where the possible locations for an S might be and finally, part (d) gives us $T - \partial S$.

Remark 3.5. We do not expect the refinement and proof of the conjecture to be simple. The few previous works in this direction, for example Federer's [11], are rather technical in nature. Notice also that this conjecture is only necessary for a rigorous foundation to the use of the dual formulation in the computation of the flat norm decomposition. Direct optimization over rectifiable currents needs nothing from this conjecture for its justification.

A very simple example where Lipschitz forms are necessary and sufficient for optimality is the case in which the current is three equally spaced circles on a torus (see Figure 3.4). Note that the metric on the torus is chosen such that the circles are parallel. Figure 3.5 shows the f of a Lipschitz maximizing form $f(x)dy$. In the case shown of equal spacing between circles, we cannot maximize with a smooth form and a maximizing sequence must approach the form plotted in Figure 3.5. In this case, the region between the $x = 0$ and $x = a$ circles or the region between the $x = a$ and $x = 2a$ circles
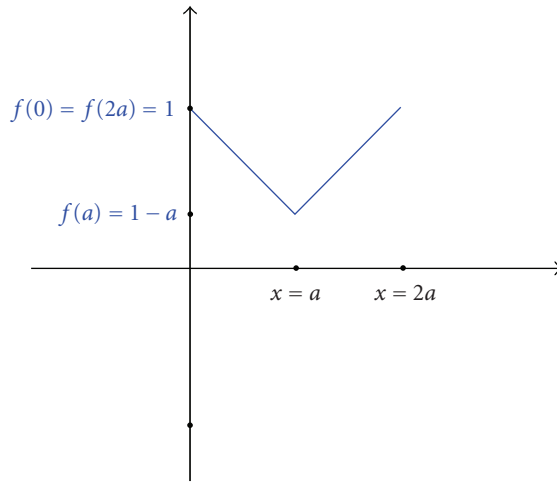
Figure 3.5. A maximizing form for the 3 circles example. We plot f for the form given by $f(x)dy$. We are forced to use $\alpha = 1$ and the Lipschitz form plotted here.

is the optimal S. This nonuniqueness is taken into account in the above conjecture. Finally, the above propositions, example, and conjecture have obvious analogs for $\mathbb{F}_\lambda$, the flat norm with scale.

3.4. L^1TV for codimension > 1. Computing the flat norm decomposition for arbitrary currents permits us to extend the L^1TV denoising to sets which are not boundaries or have codimension greater than 1. One approach is to use the dual formulation of the flat norm. This depends on extracting the optimal decomposition from the optimizing form, as discussed in the previous subsection. Another approach is to directly optimize over currents. We are currently developing both approaches. Figure 3.6 schematically illustrates the decomposition of a 1-current in 3D that results when the flat norm is computed. This example actually illustrates both of the useful generalizations possessed by the flat norm decomposition: regularization or denoising of higher codimension and non-boundary subsets. Notice that the use of the flat norm with scale permits us to choose what scale is small and therefore greatly diminished, and what scales are large and therefore preserved. In the case of sets which are codimension 1 boundaries, we know that in a very precise sense, the regularized surface given by spt$(T - \partial S)$ is the best λ-curvature approximation to T (see [2, 3] for details).

3.5. Shape statistics. As noted above, the flat norm was previously suggested for shape comparisons in [8, 9] and then used in [10] for the purpose of computing shape statistics. Our observation permits us to use L^1TV algorithms to compute the flat norm distance for many shapes in shape space and the flat norm decomposition that gives this distance. The decomposition that we get as a result shows us where the difference is big with respect to λ and where it is small (see Figure 3.7).
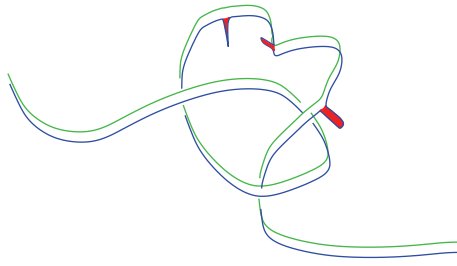
Figure 3.6. The green curve is the denoised version of the blue, where we have translated the green to make visualization easier.
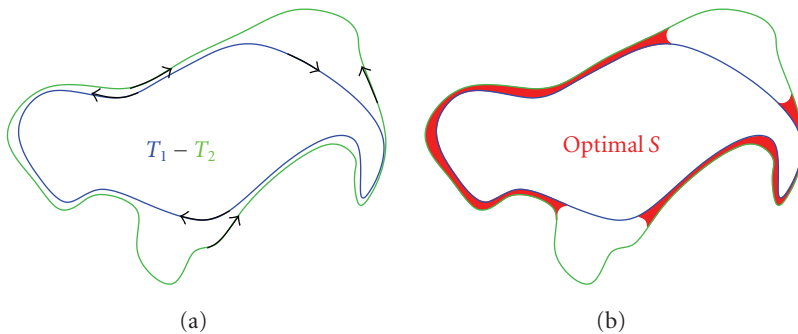

(a)

(b)

Figure 3.7. The flat norm via the L^1TV functional provides us with both a distance and an informative optimal decomposition into S and $T_1 - T_2 - \partial S$. To use L^1TV on sets, we need that $T_1 = \partial\Omega_1$ and $T_2 = \partial\Omega_2$ and either $\Omega_1 \subset \Omega_2$ or $\Omega_2 \subset \Omega_1$. Using a direct method for computing the $\mathbb{F}_\lambda$ we do not need these inclusions. Alternatively, we can identify the difference between two shapes $\partial\Omega_1$ and $\partial\Omega_2$ as the boundary of the set $\Omega_1 \triangle \Omega_2$. Then we can use L^1TV for all codimension 1, boundary shape differences, without requiring inclusions.

4. Summary

The innovations introduced in this paper simultaneously expand the methods available for computing L^1TV minimizers, generalizes L^1TV to nonboundary and higher codimensional subsets, opens up a new method for multiscale shape decompositions, and supports the previous suggestion of Glaunès et al. that the flat norm is useful as a distance in shape space.

Difficulties include the fact that nonboundary 0-currents, that is, sets of signed points in $\mathbb{R}^n$ not arising as the endpoints of a family of curves, seem rather clumsy to handle. For some applications the global curvature bound enforced by the method might be too limiting. One can imagine a situation in which the curvature of the approximation should be allowed to vary from place to place on the input current or set. One might in fact desire something that returns a denoised set whose use as a local mean generates a local variance inversely proportional to the locally allowed curvature.

It is not as easy to handle noise in T in the form of gaps or missing pieces of T. Of course, missing pieces means that T is not a boundary. One approach is to first denoise ∂T and then add the resulting S to T to fill in many or all of the gaps. Then $T + S$ can be denoised to remove oscillations by computing the optimal $\mathbb{F}_\lambda$ decomposition. But then the denoising process requires two steps, each involving a choice of λ and this seems a bit clumsy. On the other hand this might make sense scientifically since the process by which holes and oscillations are generated may be quite different with different associated length scales.

In conclusion the program suggested by the relatively simple observation of the relation between L^1TV and the flat norm promises many new benefits. Many of these benefits are immediately accessible while others depend on the some further developments outlined above. These, as well as the general expansion of the above announcement is the subject of several papers that are in preparation or in planning with collaborators.

Appendix

Micro tutorial on currents and the flat norm

If you know something about currents and have a clear picture of the flat norm, this section can be skipped. The reference for this section is Frank Morgan's nice introduction [12]. The definitive, though formidable, treatise for a fair bit of geometric measure theory is still Federer's 1969 tome [13]. References between Morgan and Federer include [14, 15].

Rectifiable sets. Let $\mathcal{H}^n$ denote n-dimensional Hausdorff measure. An n-rectifiable subset N of $\mathbb{R}^{n+k}$ is the union of (1) an $\mathcal{H}^n$ negligible set and (2) a countable collection of subsets of C^1 n-submanifolds of $\mathbb{R}^{n+k}$. We are often interested in the case where $\mathcal{H}^n(N) < \infty$. Intuitively, an n-rectifiable set looks a great deal like an n-manifold at most of its points.

Currents. n-Currents in $\mathbb{R}^{n+k}$, denoted $\mathcal{D}_n(\mathbb{R}^{n+k})$, are the duals to $\mathcal{D}^n(\mathbb{R}^{n+k})$, the smooth, compactly supported n-forms on $\mathbb{R}^{n+k}$. We will usually suppress the $\mathbb{R}^{n+k}$ and refer simply to $\mathcal{D}_n$ and $\mathcal{D}^n$. We restrict ourselves to integer multiplicity rectifiable currents T, which have the following representation: $T(\phi) = \int_N \Theta(x)\langle\phi(x),\xi(x)\rangle d\mathcal{H}^n$, for all $\phi \in \mathcal{D}^n$ where N is an n-rectifiable set in $\mathbb{R}^{n+k}$, $\Theta(x)$ is an integer multiplicity density function, always ± 1 in this paper, ϕ is the form T is operating on, and $\xi(x)$ is the unit, simple n-vector defining the orientation on N. Recall that a simple n-vector is the wedge product of n vectors. In our case, $\xi(x)$ can be thought of as an oriented representation of the tangent plane to N at x. Changing the sign of the density function has the effect of reversing the orientation on N which can also be achieved by replacing ξ with $-\xi$.

Currents are naturally equipped with a boundary operator, $\partial T(\phi) \equiv T(d\phi)$. ∂T is therefore an $(n-1)$-current which operates on $(n-1)$-forms. Note the intentional consistency of this definition with Stokes' theorem.

Intuitively, a current is an oriented manifold or union of oriented manifolds, each with an oriented boundary whose orientation is inherited from the orientation of the manifold (see Figure A.1). There are of course wild beasts in the menagerie of currents, but unions of C^1 manifolds with boundary covers a great deal of ground, especially when applications are the goal.
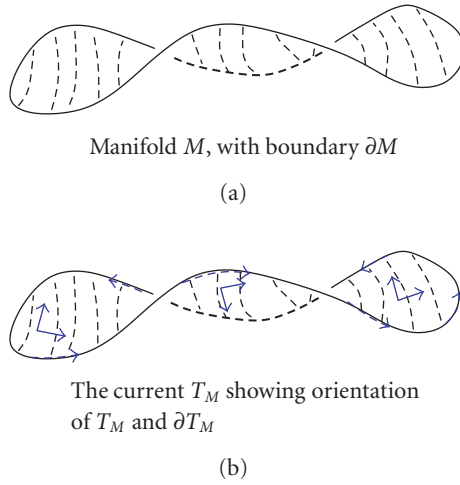
Manifold M, with boundary ∂M

(a)

The current T_M showing orientation
of T_M and ∂T_M

(b)

Figure A.1. Example 2-current T_M. Notice that $\partial T_M = T_{\partial M}$. The orientation on the boundary ∂M is simply that inherited from the orientation on M.

Mass and the flat norm.   The *mass* of a current is defined as

$$M(T) = \sup_{|\phi| \leq 1, \phi \in \mathscr{D}^n} T(\phi). \tag{A.1}$$

Informally, the *mass* is simply the n-dimensional volume of the rectifiable set carrying the n-current. By [13, Theorem 4.1.12], the *flat norm* can be defined in two equivalent ways:

$$\mathbb{F}(T) = \min_{S \in \mathscr{D}_{n+1}} \left(M(S) + M(T - \partial S) \right) \text{ (given above)},$$

$$\mathbb{F}(T) = \sup_{|\phi| \leq 1, |d\phi| \leq 1, \phi \in \mathscr{D}^n} \left(T(\phi) \right) \text{ (mentioned above)}. \tag{A.2}$$

The corresponding dual definition of the flat norm with scale is given by

$$\mathbb{F}_\lambda(T) = \sup_{|\phi| \leq 1, |d\phi| \leq \lambda, \phi \in \mathscr{D}^n} \left(T(\phi) \right). \tag{A.3}$$

Examples of the flat norm decomposition.   The flat norm involves the optimal decomposition of the n-current T into an n-current $(T - \partial S)$ and an $(n + 1)$-current S. We use the term *decomposition* in reference to the fact that $T - \partial S$ and S are the components explicitly measured by the flat norm, even though $T = (T - \partial S) + \partial S$ rather than $T = (T - \partial S) + S$ (see Figure A.2).

Examples of maximizing forms.   The dual formulation of the flat norm involves finding the supremum over appropriately constrained forms. Figure A.3 shows a maximizing
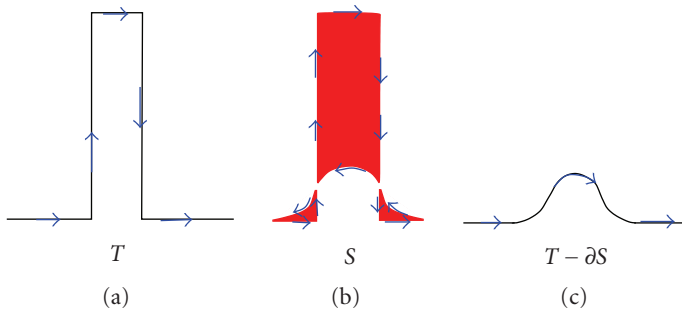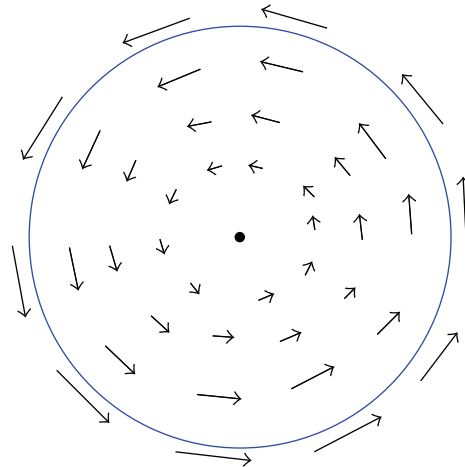
Figure A.2. Example flat norm decomposition. T is the 1-current we are computing the flat norm of, and S gives the optimal decomposition into S and $T - \partial S$. Finally, the flat norm is simply $M(S) + M(T - \partial S)$ = length of the right-most curve and area of the red region.

Maximizing form ϕ for disk of radius r

$$\phi = \frac{x}{r}dy - \frac{y}{r}dx$$

Figure A.3. A maximizing form for the disk in 2D. This form satisfies the constraints as long as $2/r \leq \lambda$. The λ is, of course, the scale in the *flat norm with scale* introduced above.

form for the 2-dimensional disk of radius r. We will discuss the computation of optimizing forms and the extraction of S from those optimizing forms in Section 3.3

Relation of the flat norm to L^1. The flat norm is very much like the L^1 norm for small differences between currents. The value of the flat norm of a difference between two currents ends up being roughly the L^1 difference between the close parts plus the sum of the n-volumes of what is left (see Figure A.4).
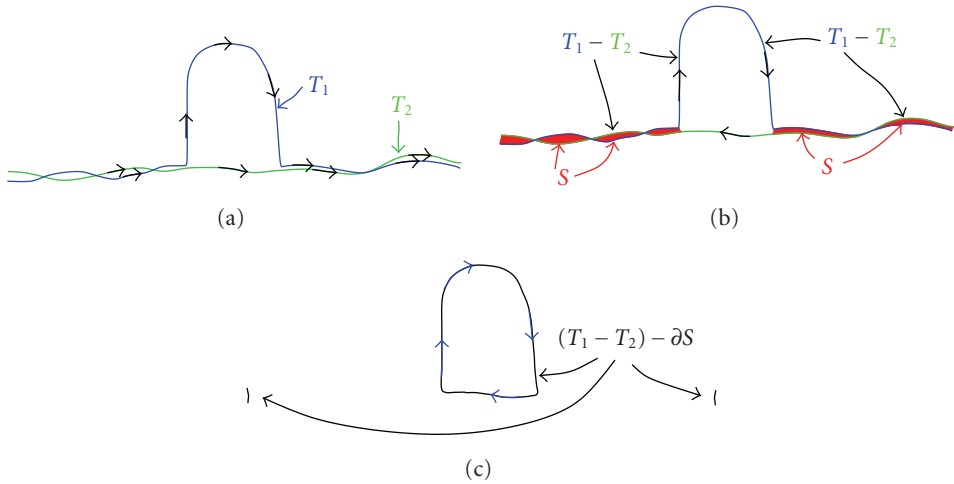
Figure A.4. The flat norm of the difference between these two currents is the sum of the area of red region (L^1 like) and the length of the loop that is left.

Acknowledgments

References

[1] T. F. Chan and S. Esedoḡlu, "Aspects of total variation regularized L^1 function approximation," *SIAM Journal on Applied Mathematics*, vol. 65, no. 5, pp. 1817–1837, 2005.

[2] K. R. Vixie and S. Esedoḡlu, "Some properties of minimizers for the L^1TV functional," preprint, 2007.

[3] W. K. Allard, "On the regularity and curvature properties of level sets of minimizers for denoising models using total variation regularization—I: theory," preprint, 2006.

[4] W. Yin, D. Goldfarb, and S. Osher, "Image cartoon-texture decomposition and feature selection using the total variation regularized L^1 functional," submitted to *SIAM Multiscale Modeling & Simulation*.

[5] S. Alliney, "A property of the minimum vectors of a regularizing functional defined by means of the absolute norm," *IEEE Transactions on Signal Processing*, vol. 45, no. 4, pp. 913–917, 1997.

[6] M. Nikolova, "Minimizers of cost-functions involving nonsmooth data-fidelity terms. Application to the processing of outliers," *SIAM Journal on Numerical Analysis*, vol. 40, no. 3, pp. 965–994, 2002.

[7] L. I. Rudin, S. Osher, and E. Fatemi, "Nonlinear total variation based noise removal algorithms," *Physica D*, vol. 60, no. 1–4, pp. 259–268, 1992.

[8] J. Glaunès, *Transport par difféomorphismes de points, de mesures et de courants pour la comparaison de formes et l' anatomie numérique*, Ph.D. thesis, l' Université Paris 13 en Mathématiques, Paris, France, 2005.

 [9] M. Vaillant and J. Glaunès, "Surface matching via currents," in *Proceedings of the 19th International Conference on Information Processing in Medical Imaging (IPMI '05)*, vol. 3565 of *Lecture Notes in Computer Science*, pp. 381–392, Springer, Glenwood Springs, Colo, USA, July 2005.

[10] J. Glaunès and S. Joshi, "Template estimation form unlabeled point set data and surfaces for computational anatomy," to appear in *Journal of Mathematical Imaging and Vision*.

[11] H. Federer, "Real flat chains, cochains and variational problems," *Indiana University Mathematics Journal*, vol. 24, no. 4, pp. 351–407, 1974.

[12] F. Morgan, *Geometric Measure Theory: A beginner's Guide*, Academic Press, San Diego, Calif, USA, 3rd edition, 2000.

[13] H. Federer, *Geometric Measure Theory*, Die Grundlehren der mathematischen Wissenschaften, Band 153, Springer, New York, NY, USA, 1969.

[14] F. Lin and X. Yang, *Geometric Measure Theory—An Introduction*, vol. 1 of *Advanced Mathematics (Beijing/Boston)*, Science Press, Beijing, China; International Press, Boston, Mass, USA, 2002.

[15] L. Simon, *Lectures on Geometric Measure Theory*, vol. 3 of *Proceedings of the Centre for Mathematical Analysis, Australian National University*, Australian National University, Centre for Mathematical Analysis, Canberra, Australia, 1983.

Simon P. Morgan: Department of Mathematics, University of Minnesota, Minneapolis, MN 55455, USA
Email address: morga084@gmail.com

Kevin R. Vixie: Los Alamos National Laboratory, Los Alamos, NM 87545, USA
Email address: vixie@speakeasy.net